Mon. Not. R. Astron. Soc. **391,** 793–801 (2008) doi:10.1111/j.1365-2966.2008.13912.x

Estimation of the tilt of the stellar velocity ellipsoid from RAVE and implications for mass models

A. Siebert,[1,2]★ O. Bienaymé,[1] J. Binney,[3] J. Bland-Hawthorn,[4] R. Campbell,[2,5] K. C. Freeman,[6] B. K. Gibson,[7] G. Gilmore,[8] E. K. Grebel,[9] A. Helmi,[10] U. Munari,[11] J. F. Navarro,[12] Q. A. Parker,[4,5] G. Seabroke,[13,8] A. Siviero,[11] M. Steinmetz,[2] M. Williams,[2,6] R. F. G. Wyse[14] and T. Zwitter[15]

[1]*Université de Strasbourg, Observatoire Astronomique, Strasbourg, France*
[2]*Astrophysikalishes Institut Potsdam, Potsdam, Germany*
[3]*Rudolf Peierls Centre for Theoretical Physics, Oxford*
[4]*Anglo-Australian Observatory, Sydney, Australia*
[5]*Macquary University, Sydney, Australia*
[6]*Australian Natianal University, Canberra, Australia*
[7]*University of Central Lancashire, Preston*
[8]*Institute of Astronomy, Cambridge*
[9]*Astronomisches Rechen-Institut, Zentrum für Astronomie der Universität Heidelberg, Heidelberg, Germany*
[10]*Kapteyn Astronomical Institut, Groningen, the Netherlands*
[11]*Astronomical Observatory of Padova in Asiago, Asiago, Italy*
[12]*University of Victoria, Victoria, Canada*
[13]*e2v Centre for Electronic Imaging, Planetary and Space Sciences Research Institute, The Open University, Milton Keynes*
[14]*Johns Hopkins University, Baltimore, MD, USA*
[15]*Faculty of Mathematics and Physics, University of Ljubljana, Ljubljana, Slovenia*

Accepted 2008 September 2. Received 2008 August 28; in original form 2008 August 7

ABSTRACT

We present a measure of the inclination of the velocity ellipsoid at 1 kpc below the Galactic plane using a sample of red clump giants from the RAdial Velocity Experiment (RAVE) Data Release 2. We find that the velocity ellipsoid is tilted towards the Galactic plane with an inclination of $7\overset{\circ}{.}3 \pm 1\overset{\circ}{.}8$. We compare this value to computed inclinations for two mass models of the Milky Way. We find that our measurement is consistent with a short scalelength of the stellar disc ($R_{\rm d} \simeq 2$ kpc) if the dark halo is oblate or with a long scalelength ($R_{\rm d} \simeq 3$ kpc) if the dark halo is prolate. Once combined with independent constraints on the flattening of the halo, our measurement suggests that the scalelength is approximately halfway between these two extreme values, with a preferred range 2.5–2.7 kpc for a nearly spherical halo. Nevertheless, no model can be clearly ruled out. With the continuation of the RAVE survey, it will be possible to provide a strong constraint on the mass distribution of the Milky Way using refined measurements of the orientation of the velocity ellipsoid.

Key words: stars: kinematics – galaxy: fundamental parameters – galaxy: kinematics and dynamics.

1 INTRODUCTION

Our understanding of Galactic stellar populations and kinematics makes regular progress with the advent of new large Galactic stellar surveys providing distances, photometry, radial velocities or proper motions. Our Galaxy is, at present, the only place where we can probe the 6D phase space of stellar positions and velocities. For instance, the Galactic 3D potential can be probed through the orbits of the Sagittarius stream (Ibata et al. 2001; Newberg et al. 2002; Helmi 2004; Read & Moore 2005; Fellhauer et al. 2006) or Palomar 5 tidal tails (Odenkirchen et al. 2003; Grillmair & Dionatos 2006; Grillmair & Johnson 2006) or through the kinematics of halo stars (Battaglia et al. 2005). At smaller scales, the potential can also be analysed through the force perpendicular to the galactic plane (Oort 1960; Kuijken & Gilmore 1989a,b,c, 1991; Crézé et al. 1998; Siebert, Bienaymé & Soubiran 2003; Holmberg & Flynn 2004) or through the coupling between the three

★E-mail: siebert@astro.u-strasbg.fr

components of the velocity in the solar neighbourhood (Bienaymé 1999).

Here, we concentrate on the question of the orientation of the velocity ellipsoid that is known to be tightly related to the shape and symmetry of the galactic potential (Lynden-Bell 1962; Ollongren 1962; Hori & Lui 1963; Amendt & Cuddeford 1991).

In spite of the long interest in this problem, measuring observationally the orientation of the velocity ellipsoid outside of the galactic plane has proven to be very difficult. This is due mainly to the absence of reliable distances away from the Solar neighbourhood. Despite this limitation, the first stellar stream detected within the Milky Way halo towards the north Galactic pole by Majewski, Munn & Hawley (1996) shows a velocity tilt, the ellipsoid being inclined towards the Galactic plane. This tilt could result from the expected velocity correlation induced by a spheroidal potential if these stars had similar integrals of motion (Bienaymé 1998). However, we note that this stream is not detected locally in the RAdial Velocity Experiment (RAVE) data (Seabroke et al. 2008).

Building realistic Galactic potentials shows that the main axis of the velocity ellipsoid, at 1 kpc above the Galactic plane, points in the direction of the *z*-axis of symmetry of the Galaxy towards a point located at 5 to 8 kpc behind the Galactic centre: for instance from numerical orbit computations (Binney 1983; Kuijken & Gilmore 1989a) or applying to the Carlberg & Innanen (1987) Galactic potential the Amendt & Cuddeford (1991) formulae. Such estimates of the velocity ellipsoid tilt are necessary for an accurate determination of the asymmetric drift[1] (Binney & Tremaine 1987), and for a correct measurement of the force perpendicular to the Galactic plane (Statler 1989).

In this paper, we study the 2D velocity distribution perpendicular to the Galactic plane for a sample of red clump stars from the RAVE survey (Steinmetz et al. 2006; Zwitter et al. 2008). These stars are selected between 500 and 1500 pc below the Galactic plane and provide a measurement of the tilt of the velocity ellipsoid at $\simeq$1 kpc. In Section 2, we present the selection of the sample while Section 3 focuses on the measurement of the inclination and possible biases. Finally, in Section 4 we compare our measurement to computed inclinations for two extreme classes of mass models and we discuss possible outcomes of this measurement.

2 SELECTION OF THE SAMPLE

Our sample is drawn from the second data release of the RAVE survey (Zwitter et al. 2008) containing about 50 000 stellar radial velocities and 20 000 measurements of stellar parameters. We focus on red clump giants towards the South Galactic pole to maximize the distance from the plane and to minimize the interstellar extinction. Hence, we select our targets in a cone with $b < -60^\circ$, and we use a colour–magnitude criterion following Veltz et al. (2008) to select our candidate red clump stars: Two-Micron All-Sky Survey (2MASS) $J - K$ colour within 0.5–0.7 and $K < 9.3$.

This colour–magnitude cut selects mainly red clump stars whose luminosity function (LF) is well defined and approximately Gaussian: $M_K = -1.6 \pm 0.03$. Also, the red clump LF is narrow, the dispersion of the Gaussian LF being 0.22 mag in the *K* band, and nearly independent of the metallicity (Alves 2000). It makes this population particularly suited to study the kinematics of stars away from the solar neighbourhood as reliable distance estimates can be obtained. Also the extinction in the *K* band remains low, $\langle A_K \rangle = 0.007$ mag with a maximum extinction of $A_K = 0.05$ mag for this region of the sky (Schlegel, Finkbeiner & Davis 1998). Hence, extinction does not contribute significantly to our error budget: the average error on the distance is less than 1 per cent with a maximum value of $\sim$2 per cent for the limiting magnitude of our sample.

The selection criterion, retaining only the objects with a proper motion value in the RAVE catalogue, restricts the sample to 763 red clump candidates spanning a distance interval from the Sun of 500 to 1500 pc. A small fraction of these selected stars are dwarfs or subgiants. According to the photometric and kinematic modelling of the SGP and NGP by Veltz et al. (2008), we can estimate that, at the limiting magnitude of our sample $M_K = 9.3$, 75 per cent of the sample are red clump stars, 10 per cent dwarfs and 15 per cent subgiants. Brighter than this limit, the fraction of red clump stars is larger and the quoted fractions are upper limits to our contamination fraction.

We clean our sample further using a kinematic selection. We select stars based on their velocities with the following criteria $\sqrt{U^2 + V^2 + W^2} < 200$ and $V < 100\,\mathrm{km\,s^{-1}}$. This selection enables us to remove the nearby dwarfs whose distance is overestimated by a factor of 14 due to their fainter absolute magnitude, hence an overestimation of their velocities. The resulting sample contains 580 red clump candidates in the direction of the South Galactic pole whose distribution in velocity space is presented in Fig. 1. In this figure, the contours depict the distribution of the original sample smoothed by the individual errors while the dots show the location in velocity space of the remaining 580 stars after the velocity selection.

We test our selection criteria using the second year observation from the RAVE survey (as a reminder, RAVE Data Release 2 (DR2) contains the first year of observation – i.e. DR1 – and the second year of observation). For these objects, RAVE provides the measurements of the stellar parameters including an estimate of the gravity. The sample selected from second year data contains 294 stars with $\log g$ measurements, with 231 stars matching the velocity criteria. The histograms of $\log g$ for each subsample are presented in Fig. 2, where the black histogram presents the distribution of $\log g$ for the 294 second year stars and the dashed histogram presents the subsample matching our velocity criteria. The red clump giants span a large range in gravity depending on their metallicity: $\log g = 2.08$ for the metal-poor, low-mass end and reaches up to $\log g = 3$ for the high-mass, metal-rich red clump objects (Zhao, Qiu & Zhang 2000). This figure clearly indicates that our velocity criteria are efficient for rejecting dwarf stars (with high $\log g$) but also remove a small fraction of stars with lower $\log g$, primarily subgiants and giants on the ascending branch and also a few red clump stars. Nevertheless, these objects have large velocities and fall in the tails of the velocity distribution. Therefore, they affect only marginally the measurement of the inclination, as our measurement is driven by the larger number of stars in the bulk of the velocity distribution.

It is worth noting that due to the uncertainties in RAVE $\log g$ measurements which are 0.5 dex for a typical RAVE star (Zwitter et al. 2008), it is not possible to obtain a firm estimate of the contamination in our sample, nor to use the RAVE $\log g$ estimates to refine our sample. Also, $\log g$ measurements are only available for less than half of our sample as stellar parameters cannot be estimated from the spectra collected during the first year of operation of RAVE. Nevertheless, considering a 0.5 dex error on $\log g$, we estimate that the contamination using the velocity criteria is reduced to

[1] The asymmetric drift is the tendency of a population of stars to lag behind the local standard of rest for its rotational velocity, the lag increasing as a function of age.

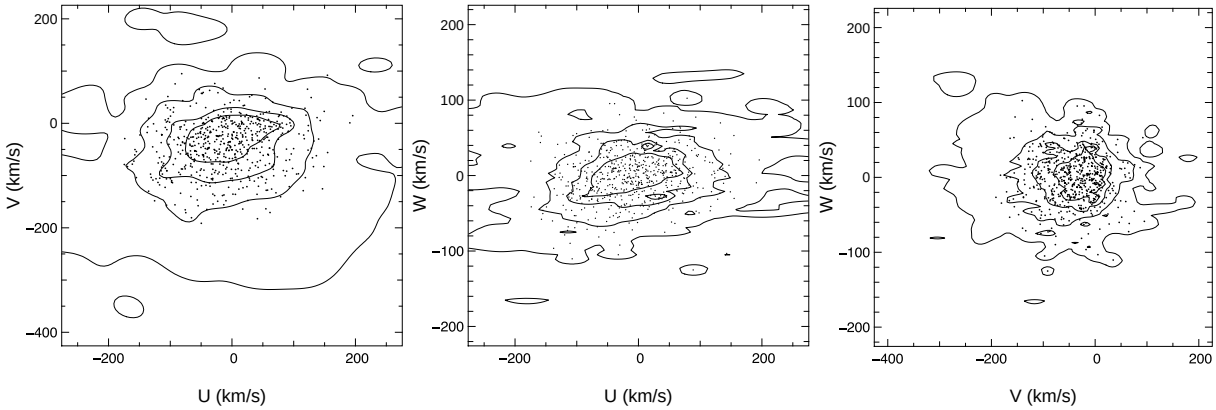

Figure 1. Selection of the red clump sample in U, V, W velocity space. The contours show the distribution of the 763 red clump candidates belonging to the original sample, smoothed by the individual errors, while the dots represent the location in the velocity space of the 580 stars in the final sample. The contours encompass 90, 70, 50 and 30 per cent of the total sample.

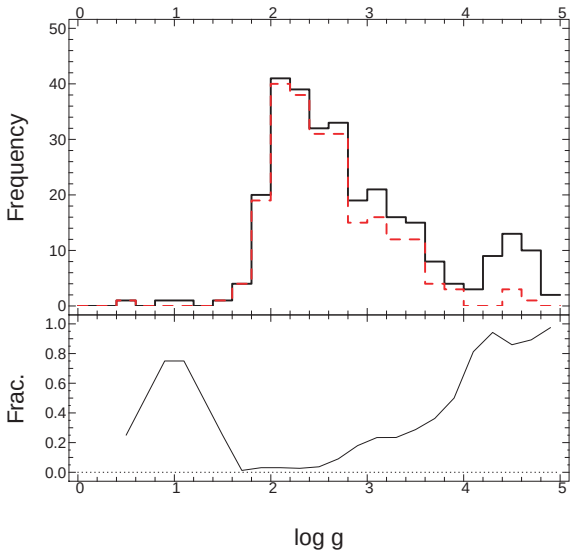

Figure 2. Top panel: histogram $\log g$ for the 294 stars with $\log g$ measurements in RAVE DR2. Black line full subsample, dashed line subsample matching the velocity criteria. The red clump giants cover the region in $\log g = 2$–3 depending on the metallicity or mass. A conservative estimate of RAVE standard error on $\log g$ is 0.5 dex. Bottom panel: fraction of stars rejected by the velocity criterion as a function of $\log g$.

$\simeq$10 per cent which is to be compared to more than 20 per cent without the velocity criteria. We will detail the effect of this contamination on our measurement in the next section.

3 MEASURING THE TILT

The tilt angle δ of the 2D velocity distribution is given by the relation

$$\tan 2\delta = \frac{2\sigma_{UW}^2}{\sigma_U^2 \sigma_W^2}, \quad (1)$$

where $\sigma_{UW}^2, \sigma_U^2$ and σ_W^2 are the velocity distribution moments. In the local velocity coordinates, the velocity in the radial direction is given by the U component of the velocity vector (positive towards the Galactic Centre) and the vertical velocity by the W component of the vector positive towards the North Galactic pole, while the V component is positive towards the Galactic rotation (not used in equation 1).

The computation of the inclination is straightforward for a sample with small and homogeneous errors. Nevertheless, to lower the effect of foreground dwarfs and giants and the contamination due to high-velocity stars, we make use of a velocity cut-off to select our sample. In this case, as our errors in the U and V velocity directions are large, a direct measurement of the tilt angle may be subject to bias and our selection criteria must be studied as our error budget may not be dominated by the size of the sample (see Section 3.1).

Also, the local velocity ellipsoid is not a smooth distribution and clumps are present on both small and large scales in the velocity space (see e.g. Dehnen 2000; Chereul, Crézé & Bienaymé 1998; Dehnen 1998; Famaey et al. 2005). These substructures prevent determining the age–velocity dispersion relation in the U and V directions (Seabroke & Gilmore 2007) and may also influence the measured tilt angle. We will discuss the effect of such substructures on our measurement in Section 3.2.

Finally, if our selection criterion is efficient at rejecting the foreground stars, only the tails of the velocity distribution are affected by the velocity cut-off. As their space velocities are overestimated, such foreground objects will impact on the measurement of the inclination. We will discuss this particular point in Section 3.3.

3.1 The effect of errors and velocity cut-off

Our velocity errors in the cardinal directions are not homogeneous because the U and V components of the velocity vector are dominated by the proper motion contribution while the W component is primarily measured from the RAVE radial velocity. Fig. 3 presents the distribution of errors for our sample in the U, V and W components as full, dashed and dotted lines. It is clear that the mode of the velocity error distributions for the U and W components, the ones we are primarily interested in, differ by a factor of 4: $\simeq$5 km s^{-1} for the W component while for the U component the distribution peaks at $\simeq$20 km s^{-1}.

This large difference results in an anisotropic smoothing of the observed velocity ellipsoid which, combined with our velocity criterion, biases the measurement of the inclination towards a lower value. This bias is due to the structure of equation (1) where the error anisotropy results in an extra component E on measured velocity dispersions. If we consider only the extra term on the U

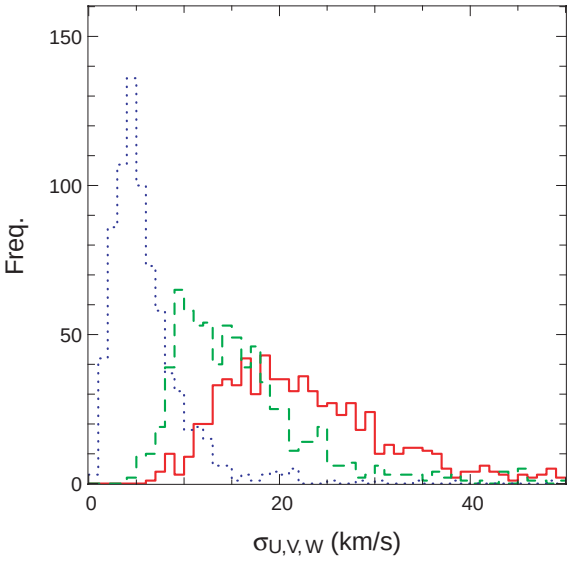

Figure 3. Distribution of the velocity errors in our sample; full line U component, dashed line V component, dotted line W component. The difference between these three distributions arises due to the relative contribution of proper motion and distance errors to the radial velocity errors for the velocities along the three cardinal directions.

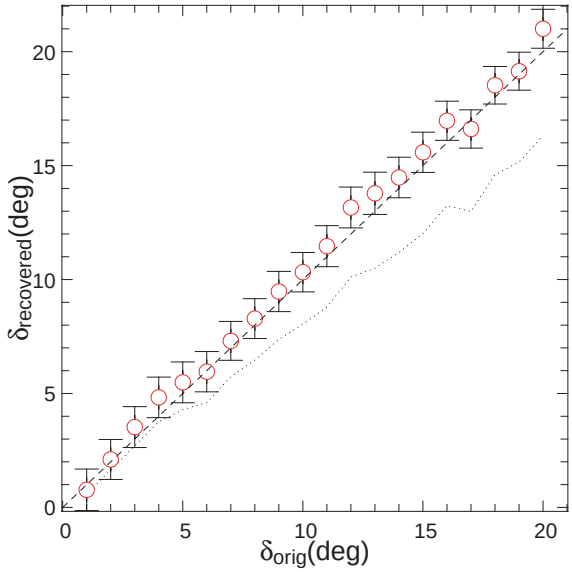

Figure 4. Test of the Monte Carlo method to measure the tilt angle of the velocity ellipsoid. The original versus recovered tilt angle are presented for one realization of a velocity ellipsoid having $\sigma_U = 31$ and $\sigma_W = 17\,\mathrm{km\,s^{-1}}$ and sampled using 1000 data points. The RAVE error laws for the velocities are used. The dashed line shows the one-to-one relation while the dotted line is a direct measurement using equation (1). The results from the Monte Carlo sampling of the error laws are depicted by the open circles and the error bars are the standard deviation of 5000 resampling for each value of the tilt angle.

component, we have $\sigma_U(\mathrm{measured})^2 = \sigma_U(\mathrm{true})^2 + E^2$ and the cross-term $\sigma_{UW}(\mathrm{measured}) = \rho_{UW}\sigma_W\sqrt{\sigma_U(\mathrm{true})^2 + E^2}$, ρ_{UW} being the correlation coefficient. With this notation, it is clear that the contribution of the additional error term is larger for the denominator than it is for the numerator, hence producing an underestimate of the true inclination. For comparison, a linear fit would not be biased due to the asymmetry of the errors but unfortunately it is more sensitive to outliers. To overcome this problem, we use a Monte Carlo sampling of the velocity error distributions. We add a random velocity term to the V and W components, degrading the accuracy of the two velocity components, so that the resulting error distributions match the U velocity error distribution. For the U velocity, it is randomly drawn from its original error distribution. This procedure enables us to obtain isotropic error distributions for all three components, degrading the two best distributions to the level of the least accurate distribution. The inclination is then computed using equation (1) after applying the velocity criterion.

We tested this procedure on a simple velocity ellipsoid model using the RAVE error laws and standard velocity dispersions for the Galactic old disc population, leaving aside the thick disc: $\sigma_U = 31$ and $\sigma_W = 17\,\mathrm{km\,s^{-1}}$. The size of the sample was set to 1000 data points and we varied the inclination of the ellipsoid from 1 to 20°. The results of this test are shown in Fig. 4 where the direct measurement is presented as a dotted line and the Monte Carlo determinations by the open circles with error bars for one random realization of a velocity ellipsoid. The one-to-one relation between the original and recovered angles is sketched by the dashed line. Below 2–4° for the inclination, depending on the realization of the ellipsoid, both methods predict the same inclination but above this threshold, the Monte Carlo sampling recovers the proper value of the angle. On the other hand, the direct measurement, applying equation (1), always underestimates the true angle with a bias rising with the tilt value. This test clearly indicates that the Monte Carlo sampling of the errors is best suited to measure the tilt of the velocity ellipsoid, while direct measurements using equation (1) are subject to strong bias in the case of heterogeneous error laws. We also note that the value of the bias depends strongly on the random sampling of the ellipsoid, with a bias varying between 2 and 4° at 7°. This spread in the bias value becomes larger as the tilt value increases and indicates that even with a proper model to estimate the bias, it can hardly be used to correct the direct measurement.

The procedure is then applied on the RAVE sample and the result is presented in Fig. 5 which shows the distribution of inclinations in degrees obtained by sampling the error distribution 25 000 times. The mean inclination measured is 7.°3 with a standard deviation of

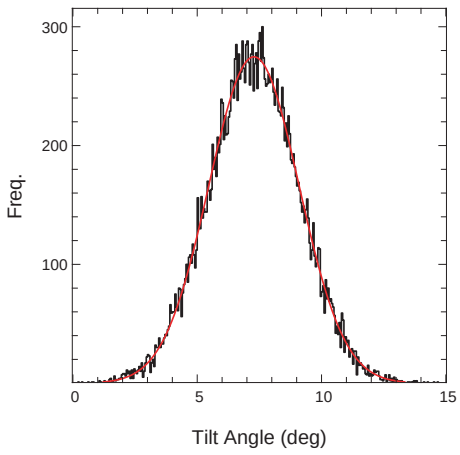

Figure 5. Distribution of the measured inclination of the velocity ellipsoid per 0.°05 bin. This distribution is obtained using a Monte Carlo sampling of the error distribution. The mean inclination is found to be 7.°3 with a standard deviation of 1.°8. The grey line is a Gaussian function with identical parameters.

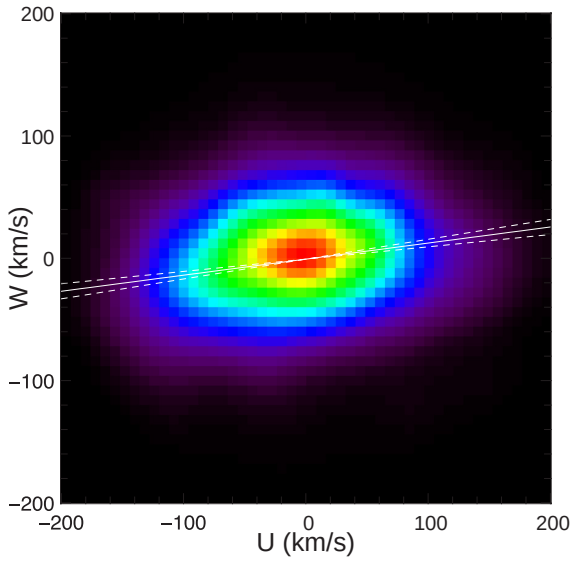

Figure 6. Velocity distribution in the (U, W) plane from our sample after sampling the error distribution. The measured inclination and 1σ range are presented by the full and dashed white line. The colour-coding follows the density per bin.

1.°8. If the anisotropy of the error distributions was not taken into account, the measured inclination would have been 6.°3 or 1.°0 too low. The 2D representation of the velocity ellipsoid inclination is shown in Fig. 6. The colour-coding follows the density of stars per bin in the region of the (U, W) space, where the 2D distribution of the (U, W) velocities has been convolved by the individual errors. The measured inclination and 1σ errors are presented as white lines (full line for the mean value and dotted lines for the errors).

3.2 Effect of substructures

Substructures such as the Hyades, Pleiades or the Hercules groups are well-known features of the local velocity ellipsoid, and are easily seen in the velocity space obtained from the *Hipparcos* mission (see e.g. Chereul et al. 1998; Dehnen & Binney 1998; Famaey et al. 2005). These structures may have a wide range of origins such as the disruption of clusters, resonances associated with the bar or spiral arms (see e.g. Dehnen 2000; De Simone, Wu & Tremaine 2004; Famaey et al. 2005; Famaey, Siebert & Jorissen 2008; Minchev & Quillen 2008). Nevertheless, the average velocity error in our sample does not allow us to distinguish these substructures.

To test the influence of these velocity substructures on the tilt determination, we use the local sample from Famaey et al. (2005). This sample provides not only accurate velocity vectors for about 6500 stars in the solar neighbourhood, it also provides an estimate of the relation of a star to the identified velocity substructures. This allows us to separate the background ellipsoid from the known overdensities.

We first estimate the fraction of stars in substructures in the Famaey et al. (2005) sample as a function of z, the height above the Galactic plane. The number of stars in structures is larger closer to the plane: 36 per cent of the stars are in structures in the 0–200 pc interval while 25 per cent are found in structures between 200 and 500 pc. This drop in number of objects in structures is sharp as seen from Table 1, the fraction in objects in structures being lowered by over a factor of 2 between 0 and 500 pc. As our sample

Table 1. Fraction and number of stars in structures in the Famaey et al. (2005) sample as a function of height above the Galactic plane.

z (pc)	$N_{\rm tot}$	Fraction in structures	Number in Hya/Plei	Number in Sirius	Number in Hercules
0–100	1361	0.40	127	63	125
100–200	1337	0.33	111	49	131
200–300	844	0.28	46	27	94
300–400	422	0.22	1	20	37
400–500	177	0.19	0	7	8

covers a distance below the plane from 500 to 1500 pc, we extrapolate this behaviour at higher z to estimate the contamination arising from substructures in our sample. Using a conservative extrapolation, we estimate the contamination in our sample to be lower than 7 per cent.

In a second step, we test the influence of the substructures on the measured inclination. We cannot use the Famaey et al. (2005) sample directly, as the presence of pertubations in the plane makes any attempt to disentangle the effect of groups from the effect of the pertubations on the inclination hazardous. Therefore, we proceed as follow. We add an additional population, drawn from a subset of the Famaey et al. sample, to our RAVE sample. This subset is randomly selected from the set of stars belonging to groups in the distance interval 300 to 500 pc. We add it to the RAVE sample varying its fraction relative to the RAVE sample from 1 to 20 per cent. This procedure enables us to mimic as closely as possible the velocity distribution of the groups, which is not homogeneous and strongly varies as a function of distance to the plane. This operation is repeated 25 000 times for each fraction of the contamination to ensure a proper coverage of the possible cases.

The results are shown in Fig. 7 where the mean deviation ($\delta_{\rm measured} - \delta_{\rm true}$) in degrees as a function of the fraction of stars in groups is drawn as a thick line. The standard deviation of the repeats is shown as dashed lines. We note that the average tilt for the Famaey

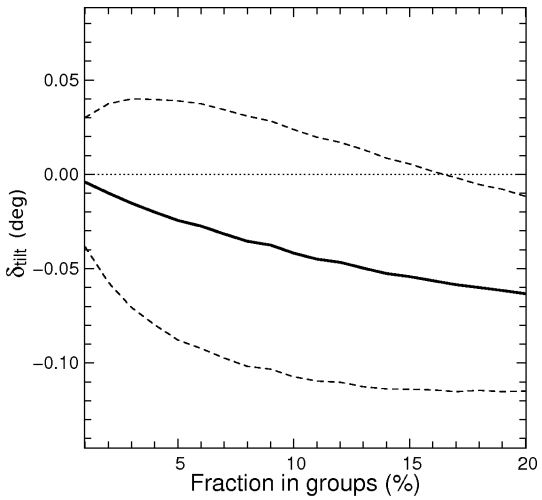

Figure 7. Influence of stars in velocity groups on the measured inclination. A sample of Famaey et al. (2005) stars belonging to groups is randomly added to the RAVE sample, varying the contamination from 1 to 20 per cent. The tilt is measured following the same procedure as for the pure RAVE sample. The thick line represents the average deviation in degrees ($\delta_{\rm tilt} = \delta_{\rm measured} - \delta_{\rm true}$) found for 25 000 repeats per contamination fraction. The dashed line is the standard deviation of the repeats.

group sample used here is 0.07 ± 2.45, very different from the value of the inclination in our sample. From this figure, we see that the influence of velocity structures on the measured tilt is low, around -0.03 for a contamination of 7 per cent with a standard deviation below 0.1. 7 per cent being an upper limit for the contamination in our sample, we do not expect groups to affect our measurement of the tilt. Indeed, the mean deviation combined with the standard deviation measured from this experiment contributes to not more than 0.1, less than 6 per cent of our estimated errors.

3.3 Effect of foreground stars

If, as we saw above, the velocity structures do not influence largely the orientation of the velocity ellipsoid, the foreground stars (dwarfs, subgiants and giants on the ascending branch) can be more problematic. The fact that their velocities are overestimated in the U direction, because of the overestimate of their distances, will add a component with low inclination to the observed ellipsoid. The bias due to these objects is an underestimate of the tilt at a given distance.

The contamination by foreground objects is about 10 per cent in our sample (see Section 2), and a factor of 14 overestimation of the U velocity for the dwarfs will render their velocity ellipsoid almost uniform in the velocity interval we consider. The velocity dispersion of this foreground population will be large, over 400 km s^{-1} instead of $\sim$31 km s^{-1} for σ_U, due to the distance overestimate. For the other sources of contamination (subgiants and giants on the ascending branch), the distance is overestimated by a factor of 2 or less, and their impact on the velocity ellipsoid is lower.

To obtain an upper limit of the effect of the foreground population, we rely on a resampling technique, replacing 10 per cent of the sample by a random realization of a thin disc population with no inclination. The overestimate of the distance is then translated into an overestimate of the velocities, and the final inclination of the velocity ellipsoid is measured applying the same procedure as above. The difference between the distribution with and without resampling provides an upper limit on the effect of foreground objects on our measurement. We note here that if adding a population with no tilt is, in principle, similar to the experiment done in Section 3.2, here we incorporate the distance overestimation. Furthermore, the added test stars are not restricted to the region in velocity space of the groups.

Fig. 8 presents the results of this resampling. The black histogram shows the distribution of the 25 000 measurements while the grey Gaussian curve is the Gaussian representation of the distribution obtained in Fig. 5. The presence of a population with no inclination does produce an observable bias in this experiment: we observe a shift of the mode of the distribution. Nevertheless, this bias is small, the measured offset is 0.15, much lower than the standard deviation of the distribution while it is a *worst-case scenario*. Indeed, here we did consider only the contamination by foreground dwarf stars while our real contamination is a mixture of dwarfs and subgiants. In the latter case, the overestimate of the distance is much lower, as these stars have a mean distance from the plane that is larger. Hence, their impact on the velocity ellipsoid orientation will be lower than for dwarfs. We also note that the presence of a foreground population renders the distribution non-Gaussian, adding a tail to the low tilt angle part of the distribution which is not observed in Fig. 5.

We can conclude that our estimate of the inclination of the velocity ellipsoid is robust and that the presence of a population of foreground objects does not introduce a significant bias in our measurement. Indeed, combining both the effect of foreground stars and the possible velocity ellipsoid substructures in a *worst-case scenario*, the resulting bias amounts to $\sim$10 per cent of our errors. At this level, the biases do not affect our conclusions.

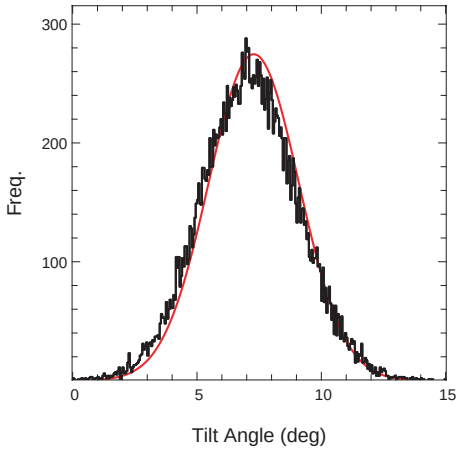

Figure 8. Results from the resampling study. 10 per cent of the red clump sample has been replaced by a population of foreground objects with no tilt and velocities in the U direction overestimated by a factor of 14. The black histogram is the distribution of measured inclination for this new sample following the same procedure as for Fig. 5 while the grey Gaussian curve is the distribution of inclination without the resampling from Fig. 5.

4 RELATION TO THE MASS DISTRIBUTION IN THE GALAXY

The tilt of the velocity ellipsoid is intimately linked to the mass distribution in the Milky Way and more specifically – if we trust our knowledge of the structure of the Galactic disc – to the flattening of the halo. We start from the mass model of Dehnen & Binney (1998)[2] and its revised parameters provided by Binney & Tremaine (2008, hereafter BT08) in their table 2.3. This revision proposes two models, referred to as models I and II, which match both local and non-local data. These models are the modified versions of the Dehnen & Binney (1998) models I and IV.

As noted in these references, a crucial parameter is the scalelength of the disc whose value lies in the range 2–3 kpc. The two models are set on the upper and lower bounds for this parameter. Model I presents a mass model with a short scalelength ($R_\mathrm{d} = 2$ kpc) that induces a strong contribution from the disc for the potential at the solar radius up to 11 kpc. On the other hand, model II has a larger scalelength ($R_\mathrm{d} = 3.2$ kpc) and therefore, the halo contribution to the rotation curve dominates at the Sun location and beyond. This is also seen from the global shape of the potential where for model II the isopotentials are more spherical than for model I (see figs 2.19 and 2.21 of BT08). For a detailed description of these two models, the reader is referred to chapter 2 of BT08.

We use both the models to discuss below the implications of the tilt on the possible models for the mass distribution in the Milky Way, focusing on the flattening of the halo in the two extreme cases. We note here that the region above (below) the plane between 1 and 2 kpc is best suited to separate the two classes of models. Indeed, in this region, the variation of the angle between the Galactic plane

[2] The Galactic potentials are computed using the GALPOT program written by W. Dehnen. This program is available within the NEMO package: http://carma.astro.umd.edu/nemo/.

Table 2. Modification to the mass models I and II of BT08 table 2.3 used in Section 4. The halo density is given in $M_\odot\,pc^{-3}$. The modified models are built, modifying the halo parameters, to keep the rotation curve almost unchanged in the disc. The bulge and disc parameters are fixed to the BT08 values.

	ρ_{halo}	
c/a	Model I	Model II
0.6	0.838	0.327
0.7	0.765	0.293
0.8	0.711	0.266
0.9	0.670	0.245
1.0	0.635	0.229
1.1	0.608	0.215
1.2	0.585	0.204
1.3	0.566	0.195
1.4	0.548	0.186
1.5	0.534	0.179
1.6	0.520	0.172
1.7	0.510	0.167

and the normal to the isopotentials as a function of the minor-to-major axis ratio c/a_ρ is maximum. Hence, we expect the difference between the predicted tilt angle to be the largest in the same region. At larger distances from the plane, the potential becomes more spherical and the difference vanishes between the models in terms of variation of the potential and inclination of the velocity ellipsoid.

To measure the tilt of the ellipsoid as a function of the halo flattening, we vary the density minor-to-major axis ratio c/a_ρ of the halo from 0.6 to 1.7 for each model, the halo density being described by the relation

$$\rho(R,z) = \rho_{\rm halo}\left(\frac{m}{a_h}\right)^{-\alpha_h}\left(1+\frac{m}{\alpha_h}\right)^{(\alpha_h-\beta_h)}, \qquad (2)$$

where the flattening c/a_ρ enters the equation through the parameter $m = \sqrt{R^2 + z^2/(c/a_\rho)^2}$, R and z being the Galactocentric cylindrical coordinates. a_h is a scale parameter with $\rho \propto m^{-\alpha_h}$ if $m \ll a_h$ and $\rho \propto m^{-\beta_h}$ for large m.

While changing c/a_ρ, we change the halo density in order to keep the rotation curve almost unchanged in the plane. The bulge and disc components are fixed to the values of table 2.3 of BT08, the solar Galactocentric radius is set to 8 kpc. Keeping the rotation curve and the disc/bulge parameters unchanged enables us to study the influence of the halo flattening on the shape of the velocity ellipsoid, as the contribution to the radial force of each component remains largely the same for each case. The corresponding density of the halo for each mass model is reported in Table 2.

The inclination of the velocity ellipsoid is computed for a given mass distribution using orbit integration. A single orbit is integrated over 30 rotations using a fourth-order Runge–Kutta algorithm. The initial conditions are drawn from a Shu distribution function matching the local data (Bienaymé 1999). For each potential, the orbit library contains over 2 million orbits from which we randomly select 10 points per orbit in the last 15 rotations. We further restrict the orbit library to data points matching the interval in R and z of the RAVE sample, this reduces the size of our final libraries to 6×10^4 to a few 10^5 points per library.

We measure the tilt using a Monte Carlo selection of the orbits, requiring that the distribution of the selected orbits matches the selection function of our RAVE sample in the (R, z) plane. Here, R is the Galactocentric radius and z is the distance above (below) the plane. This selection function is obtained by convolving the distribution of the RAVE sample in R and z by their errors for each star. This procedure ensures us that the spatial distribution in R and z of the RAVE sample is well matched by the orbit selection. We select 5000 orbits using the spatial constraints, about 10 times larger than the observed sample but about 10^2 times less than orbit library size to minimize the probability of the same orbit to be selected twice, and the tilt is measured using the associated velocities and equation (1). The measurement is repeated 500 times to obtain the mean inclination and dispersion. This procedure is repeated for each orbit library. The convergence of this procedure is tested using 1000, 5000 and 10 000 orbits points for the selection. The result shows a very good stability of the mean inclination, of the order of a few 10^{-2} degrees, while the dispersion increases as the number of orbits becomes lower. For the model I with $c/a_\rho = 1.0$, we obtain, respectively, an inclination of 9.89 ± 1.09, 9.83 ± 0.44 and 9.85 ± 0.36 for 1000, 5000 and 10 000 orbits, which indicates that the gain in precision above 5000 orbits is limited as the computing time scales linearly with the number of orbits.

The resulting measurements are presented in Fig. 9, left-hand panel where the full horizontal line is our measurement from Section 3 and the horizontal dashed lines are the 1σ limit. The two remaining curves correspond to the measurements obtained from our orbit analysis. The top curve is our prediction for the class of model I of BT08 and the bottom curve for the class of model II. For comparison, the right-hand panel presents for the direct measurement, without correcting the tilt for the velocity error anisotropy. The circles and crosses correspond to Monte Carlo realizations of the RAVE sample using the orbit libraries where the RAVE velocity errors have been applied on the orbit library directly. Circles and crosses are, respectively, for the class of models I and II. The error bars are the standard deviation of 1000 realizations.

The classes of models show the same general gross properties. The predicted tilt rises as the flattening decreases, reaching a maximum in the prolate halo region. This maximum is expected and varies depending on the details of each model. It is due to the fact that, when c/a_ρ becomes large, the potential becomes separable in cylindrical coordinates. On the other hand, if c/a_ρ approaches 0, the problem reduces to the plane-parallel case and the expected inclination at 1 kpc is $\delta \simeq 3^\circ$.

The two classes of models provide different estimates for the tilt of the velocity ellipsoid within the limits of our sample. The tilt variation versus c/a_ρ is larger for prolate models than it is for oblate models. For a density flattening of 0.6, the difference is only 2°, while for slightly prolate models the difference reaches up to 5°. Also, in the oblate case, the expected inclination rises more quickly than for the prolate case. If one compares the predictions for the two classes of models to the measured inclination, a clear tendency is present: the more massive the halo is, the more prolate it must be to match the tilt of the velocity ellipsoid at 1 kpc. The two extreme cases 'separater' around $c/a_\rho \simeq 0.9$: while for a massive disc $c/a_\rho \leq 0.9$ is necessary to reproduce the tilt, $c/a_\rho \geq 0.9$ is needed for a massive halo in the 1σ limit. More specifically, the measured orientation of the velocity ellipsoid is consistent with a short scalelength of the disc if the halo is oblate, while in the other case – a scalelength of the disc of the order of 3 kpc – the measured value for the tilt implies that the halo must be prolate.

Using a direct measurement, applying the velocity errors on Monte Carlo realization of the RAVE sample has the benefit of reducing the errors by a factor of $\sqrt{2}$ (Fig. 9, right-hand panel). Nevertheless, the bias increases with the inclination, see Fig. 4, which

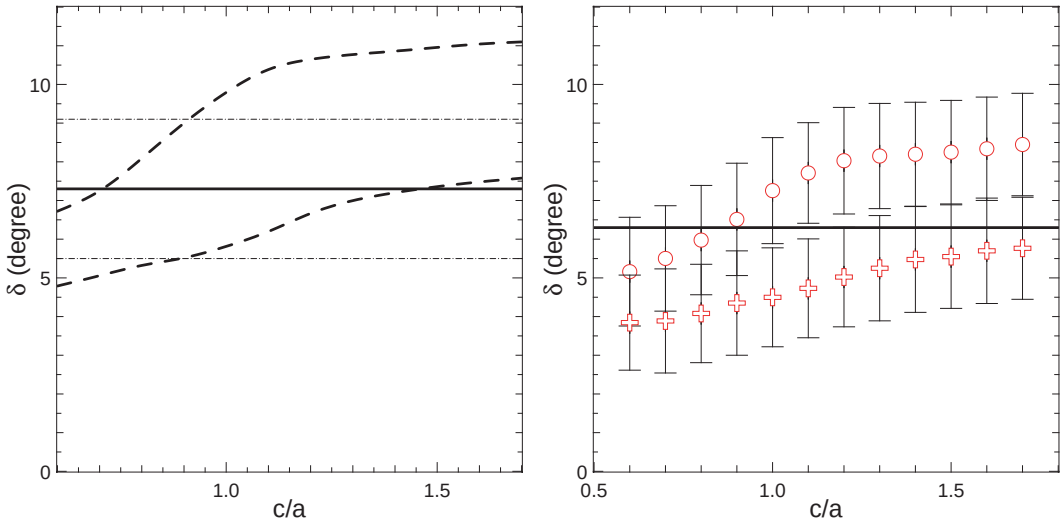

Figure 9. Left-hand panel: inclination of the velocity ellipsoid as a function of the halo flattening c/a_ρ in the RAVE selection function. The full and thin dash–dotted horizontal lines correspond to our measurement and error bars using isotropic error laws. The two dashed curves correspond to the class of models I (top panel) and II (bottom panel) in BT08 for which we varied the halo flattening. Right-hand panel: same as left-hand panel but for a direct measurement. The horizontal line is the direct measurement of the tilt without correction for the velocity error anisotropy. The circles and crosses are for Monte Carlo realization of the RAVE sample using the RAVE velocity error laws for the class of models I (circles) and II (crosses). The error bars are the standard deviation obtained from 1000 realizations.

results in the difference between the two models being lower. This direct measurement indicates that low values of c/a_ρ are marginally inconsistent with the measured tilt, with $c/a_\rho > 0.7$ being preferred even so the same general conclusions hold for both modelling technique. We note, however, that applying the errors on the orbit library (direct method) and correcting the anisotropy of the velocity errors (unbiased measurement) produces slightly different predictions for the tilt. This is partly due to the fact that the U and V velocities are computed from the knowledge of distances and proper motions. Hence, U and V errors increase with distance which is not taken into account in the Monte Carlo simulation for the direct measurement, the RAVE sample being too small to estimate properly the error laws as a function of distances. This effect is also reduced in the unbiased measurement but is still present since the correcting term is added to the true error, hence distant stars will still have on average larger errors while nearer objects will have on average smaller errors.

Further constraints on the minor-to-major axis ratio are also available from independent studies. For example, the flattening of the dark halo has been estimated from the shape of the Sagittarius dwarf tidal stream. A value $c/a_\rho > 0.7$, with a preferred flattening of $c/a_\rho \simeq 1$, is obtained by Ibata et al. (2001) and Majewski et al. (2003) using, respectively, carbon stars and M-giants from the 2MASS survey along the orbit of Sagittarius. Johnston, Law & Majewski (2005) give even stronger constraint $0.75 < c/a_\rho < 1.1$ at a 3σ level, with oblate haloes strongly favoured if precession of Sgr's orbit is considered. In contrast, Helmi (2004) and Law, Johnston & Majewski (2005) demonstrated that only Galactic potentials with prolate haloes could reproduce the velocity trends in the leading debris with a preferred axis ratio $c/a_\rho = 5/3$. However, Law et al. (2005) explored a wide variety of Galactic potentials but failed to find a single orbit that can fit both the velocity trends and the sense of precession.

Looking back at the solar neighbourhood, if the Sgr stream is orbiting in oblate and spherical potentials, Law et al. (2005) and Martinez-Delgado et al. (2007) both predict that the Sun is currently bathing in a stream of debris from Sgr, passing both inside and outside the solar circle. Models orbiting in prolate potentials are on the other hand inconsistent with this prediction. Belokurov et al. (2006), Newberg et al. (2006) and Seabroke et al. (2008) all provide strong evidence for the absence of Sgr debris in the solar neighbourhood. Fellhauer et al. (2006) argue that the origin of the bifurcation in the Sgr stream is only possible if the halo is close to spherical, as the angular difference between the branches is a measure of the precession of the orbital plane. This suggests that the absence of the Sgr stream near the Sun is consistent with nearly spherical and prolate Galactic potentials and seemingly inconsistent with oblate potentials. However, recently Ruzicka, Palous & Theis (2007) studied the Magellanic System – Milky Way interaction using test particle simulations and compared them to H I observations. They concluded that $c/a_\rho < 1$ values (oblate halo) are preferred and allow a better match to H I observations.

In Fig. 9, the preferred region by most studies, $0.75 < c/a_\rho < 1$, does not permit us to set strong constraints either on the flattening nor on the mass of the disc. The measured value of the tilt falls between the two classes of models in the allowed region, and the error bars on the RAVE measurement do not permit us to tighten the parameter space reliably. For strongly prolate haloes, as suggested by Helmi (2004), the class of model II is preferred while short disc scalelength is marginally rejected at the 2σ level. If one adopts the axis ratio $c/a_\rho = 1$ as preferred by Majewski et al. (2003) or Ibata et al. (2001), the value of the tilt is better recovered with a model whose scalelength of the disc lies in the range $R_\mathrm{d} = 2.5$–2.7 kpc. Nevertheless, at the 1σ level, large and short values for R_d are permitted with this analysis.

Various studies in the literature have used star counts to constrain the scalelength of the thin disc. For example, recently Juric et al. (2008) measured the scalelength of the stellar disc and found $R_\mathrm{d} = 2.6$ kpc (± 20 per cent) using Sloan Digital Sky Survey data. Similarly, using data from the Bologna open cluster survey (BOCCE), Cignoni et al. (2008) found a scalelength in the range 2.25–3 kpc and Ojha (2001) found 2.8 kpc using the 2MASS survey. These values

are in good agreement with our finding but have similarly large error bars. Refining our measurement will provide an independent constraint on the scalelength of the stellar disc.

5 CONCLUSIONS

We measured the tilt of the velocity ellipsoid at $\simeq$1 kpc below the Galactic plane using a sample of red clump giants from the RAVE DR2 catalogue. We find its inclination to be $7.3 \pm 1.^{\circ}8$. Estimates of the effect of contamination by foreground stars and substructures have been shown to be small and their effect on our measured value can be neglected.

We compared this value to predictions from two extreme cases of mass models for the Milky Way proposed by BT08. In the case of a massive disc with a small scalelength ($R_{\rm d} = 2$ kpc), the inclination is compatible with an oblate halo whose minor-to-major axis ratio c/a_{ρ} is lower than 0.9 at the 1σ level. On the other hand, in the case of a massive halo with large disc scalelength ($R_{\rm d} \simeq 3$ kpc), prolate haloes are preferred with $c/a_{\rho} \geq 1$. When a direct measurement is used, low values for c/a_{ρ} can be marginally rejected, indicating that $c/a_{\rho} > 0.7$.

When further independent constraints from previous studies are considered, we find that an intermediate value for the disc scalelength $R_{\rm d} \simeq 2.5$–2.7 kpc is preferred for a nearly spherical halo, but no extreme model can be clearly ruled out, due to our large error bars. This range is in good agreement with other studies relying on star count analysis and deep photometric surveys. Nevertheless, these results have large error bars of the same order of as our measurement and cannot be used to further constrain the mass distribution.

RAVE continues to acquire spectra and this work relies on the second data release of the survey. So far, RAVE has collected more than 200 000 spectra, four times the size of the sample used here. With the current observing rate, we can expect to multiply by 10 the size of our sample in the coming years which will allow us to significantly reduce our error bars. By the end of the survey, we will be able to provide a new mass model for the Milky Way galaxy with a constrained scalelength of the disc and minor-to-major axis ratio of the dark halo.

ACKNOWLEDGMENTS

AS would like to thank the anonymous referee for a very constructive report and his comments that helped clarify this paper. Funding for RAVE has been provided by the Anglo-Australian Observatory, the Astrophysical Institute Potsdam, the Australian Research Council, the German Research foundation, the National Institute for Astrophysics at Padova, The Johns Hopkins University, the Netherlands Research School for Astronomy, the Natural Sciences and Engineering Research Council of Canada, the Slovenian Research Agency, the Swiss National Science Foundation, the National Science Foundation of the USA (AST-0508996), the Netherlands Organization for Scientific Research, the Particle Physics and Astronomy Research Council of the UK, Opticon, Strasbourg Observatory and the Universities of Basel, Cambridge, and Groningen. The RAVE web site is at www.rave-survey.org.

REFERENCES

Alves D., 2000, ApJ, 539, 732
Amendt P., Cuddeford P., 1991, ApJ, 368, 79
Battaglia G. et al., 2005, MNRAS, 364, 433
Belokurov V. et al., 2006, ApJ, 642, L137
Bienaymé O., 1998, in McLean B. J., Golombek D. A., Hayes J. J. E., Payne H. E., eds, Proc. IAU Symp. 179, New Horizons from Multi-Wavelength Sky Surveys. Kluwer, Dordrecht, p. 209
Bienaymé O., 1999, A&A, 341, 86
Binney J., 1983, in Philip A. G. D., Upgren A. R., eds, Proc. IAU Colloq. 76, The Nearby Stars and the Stellar Luminosity, p. 259
Binney J., Tremaine S., 1987, Galactic Dynamics. Princeton Univ. Press, Princeton, NJ
Binney J., Tremaine S., 2008, Galactic Dynamics. Princeton Univ. Press, Princeton, NJ (BT08)
Carlberg R. G., Innanen K., 1987, ApJ, 94, 666
Cignoni M., Tosi M., Bragaglia A., Kalirai J. S., Davis D. S., 2008, MNRAS, 386, 2235
Crézé M., Chereul E., Bienaymé O., Pichon C., 1998, A&A, 329, 920
Caldwell J. A. R., Ostriker J. P., 1981, ApJ, 251, 61
Chereul E., Crézé M., Bienaymé O., 1998, A&A, 340, 384
Dehnen W., 1998, AJ, 115, 2384
Dehnen W., 2000, AJ, 119, 800
Dehnen W., Binney J., 1998, MNRAS, 294, 429
De Simone R., Wu X., Tremaine S., 2004, MNRAS, 350, 627
Famaey B., Jorissen A., Luri X., Mayor M., Udry S., Dejonghe H. T. C., 2005, A&A, 430, 165
Famaey B., Siebert A., Jorissen A., 2008, A&A, 483, 453
Fellhauer M. et al., 2006, ApJ, 651, 167
Grillmair C. J., Dionatos O., 2006, ApJ, 641, L37
Grillmair C. J., Johnson R., 2006, ApJ, 639, L17
Helmi A., 2004, ApJ, 610, L97
Holmberg J., Flynn C., 2004, MNRAS, 352, 440
Hori L., Liu T., 1963, PASJ, 15, 100
Ibata R., Lewis G. F., Irwin M., Totten E., Quinn T., 2001, ApJ, 551, 294
Johnston K. V., Law D. R., Majeswki S. R., 2005, ApJ, 619, 800
Juric M. et al., 2008, ApJ, 673, 864
Kuijken K., Gilmore G., 1989a, MNRAS, 239, 571
Kuijken K., Gilmore G., 1989b, MNRAS, 239, 605
Kuijken K., Gilmore G., 1989c, MNRAS, 239, 651
Kuijken K., Gilmore G., 1991, ApJ, 367, L9
Law D. R., Johnston K. V., Majewski S. R., 2005, ApJ, 619, 807
Lynden-Bell D., 1962, MNRAS, 124, 95
Majewski S. R., Munn J. A., Hawley S. L., 1996, ApJ, 459, L73
Majewski S. R., Skrutskie M. F., Weinberg M. D., Ostheimer J. C., 2003, ApJ, 599, 1082
Martinez-Delgado D., Peñarrubia J., Jurić M., Alfaro E. J., Ivezić Z., 2007, ApJ, 660, 1264
Minchev I., Quillen A. C., 2008, MNRAS, 386, 1579
Newberg H. J. et al., 2002, ApJ, 569, 245
Newberg H. J., Yanni B., Cole N., Beers T. C., Re Fiorentin P., Schneider D. P., Wilhelm R., 2006, ApJ, 668, 221
Odenkirchen M. et al., 2003, AJ, 126, 2385
Ojha D. K., 2001, MNRAS, 322, 426
Ollongren A., 1962, BAAS, 16, 561
Oort J. H., 1960, BAAS, 15, 45
Olling R. P., Merrifield M. R., 2001, MNRAS, 326, 164
Read J. I., Moore B., 2005, MNRAS, 361, 971
Ruzicka A., Palous J., Theis C., 2007, A&A, 461, 155
Schlegel D. J., Finkbeiner D. P., Davis M., 1998, ApJ, 500, 525
Seabroke G. M., Gilmore G., 2007, MNRAS, 380, 1348
Seabroke G. M. et al., 2008, MNRAS, 384, 11
Siebert A., Bienaymé O., Soubiran C., 2003, A&A, 399, 531
Statler T. S., 1989, ApJ, 344, 217
Steinmetz M. et al., 2006, AJ, 132, 1645
Veltz L. et al., 2008, A&A, 480, 753
Zhao G., Qiu H.-M., Zhang H.-W., 2000, AcApS, 20, 389
Zwitter T. et al., 2008, AJ, 136, 421

This paper has been typeset from a TEX/LATEX file prepared by the author.